

Multilaminate piezoelectric PVDF actuators to enhance performance of soft micro robots

Nicholas Gunter¹, Heiko Kabutz¹, Kaushik Jayaram^{1,*}

Abstract—Multilayer piezoelectric polyvinylidene fluoride (PVDF) actuators are a promising approach to enhance performance of soft microrobotic systems. In this work, we develop and characterize multilayer PVDF actuators with parallel voltage distribution across each layer, bridging a unique design space between brittle high-force PZT stacks and compliant but lower-bandwidth soft polymer actuators. We show the effects of layer thickness and number of layers in actuator performance and their agreement with a first principles model. By varying these parameters, we demonstrate actuators capable of >3 mm of free deflection, >20 mN of blocked force, and ≥ 500 Hz, while operating at voltages as low as 150 volts. To illustrate their potential for robotic integration, we integrate our actuators into a planar, translating microrobot that leverages resonance to achieve locomotion with robustness to large perturbations.

I. INTRODUCTION

Piezoelectric actuators are widely utilized at small scales due to their intrinsic electromechanical coupling, enabling precise, rapid, and controllable motion with integrated sensing capability. For micro-robotic flight [1], [2] and walking [3]–[5], piezoelectric actuators utilize lead zirconate titanate (PZT) ceramics. These exhibit high piezoelectric coefficients ($d_{31} \sim -85$ pm/V), large electromechanical coupling factors ($k_{33} \sim 0.6$ – 0.75), and operational bandwidths extending into the hundreds of kilohertz [6]. These attributes make PZT stacks and bimorphs the standard for nanopositioning, adaptive optics, and ultrasonic systems. However, their brittleness, limited strain ($< 0.3\%$), and high density (~ 7.6 g/cm³) restrict their suitability for mobile microrobotics, where actuators must endure impacts, conform to complex geometries, and operate reliably under dynamic loading [7]. As a result, PZT-based actuators can be unreliable in dynamic or uncertain environments.

Soft electroactive polymer actuators, including shape memory polymers (SMPs), dielectric elastomer actuators (DEAs) [8] and hydraulically amplified self-healing electrostatic (HASEL) actuators [9], [10], address some of these limitations. DEAs and HASELs can achieve strains exceeding 100% and demonstrate among the highest specific work densities of any soft actuation technology [11]. However, their operation typically requires very high voltages (1–10 kV), which are impractical for most microrobotic applications,

Any opinions, findings, and conclusions or recommendations expressed in this material are those of the authors(s) and do not necessarily reflect the views of the any funding agency. This work is partially funded through grants from the Paul M. Rady Mechanical Engineering Department, US Army research office (ARO) Grant # W911NF-23-1-0039 and the Meta Foundation (K.J.).

¹Animal Inspired Movement and Robotics Laboratory, Paul M. Rady Department of Mechanical Engineering, University of Colorado Boulder

*For correspondence, kaushik.jayaram@colorado.edu

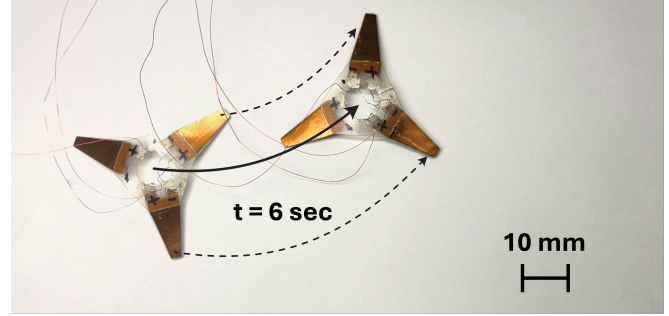


Fig. 1: PVDF actuators integrated into a robot

and their performance is limited by viscoelastic or fluidic dynamics that constrain bandwidths to 1–1000 Hz.

Poly(vinylidene fluoride) (PVDF) and its copolymers, such as P(VDF-TrFE), offer a promising middle ground between brittle PZT ceramics and high-voltage soft polymer actuators. A single layer PVDF unimorph film actuator has been used for low force soft insect scale robots [12]. PVDF is a piezoelectric polymer with a lower piezoelectric strain coefficient ($d_{31} \sim -25$ pm/V compared to ~ -85 pm/V for PZT) but compensates through several advantageous material properties:

(a) **Flexibility and robustness:** PVDF is mechanically tough and can sustain strains exceeding 2%, enabling repeated large-deflection bending without fracture.

(b) **Resonant operation:** While PZT actuators are prone to cracking under resonant excitation, PVDF actuators can operate safely at resonance, achieving up to an order-of-magnitude increase in deflection and force ($Q \sim 10$ – 15) [13].

(c) **High dielectric strength and thin-film processability:** PVDF films can withstand electric fields exceeding 100 kV/mm, enabling multilaminate architectures that achieve high electric fields at relatively low voltages (hundreds of volts).

(d) **Low density and conformability:** With a density of approximately 1.8 g/cm³, PVDF laminates are lightweight and easily integrated into flexible or curved robotic structures.

(e) **Self-sensing capability:** The inherent piezoelectric effect allows PVDF to function simultaneously as both actuator and sensor, enabling proprioceptive systems without added complexity.

In this work, we leverage these advantages to develop and characterize multilayer PVDF actuators with parallel voltage distribution across each layer [14]. Optimizing the

manufacturing process previously developed for pzt actuators [15] [16], we fabricated 4- and 8-layer devices and experimentally confirmed that blocked force and free displacement performance are predictable from first-principles models. Blocked force increases approximately linearly with the number of active layers when driven in parallel, reducing the required voltage amplitude to achieve a given output force. This multilaminate design strategy enhances force density and scalability while maintaining low driving voltage requirements, making PVDF actuators particularly compelling for microrobotic applications where stroke, robustness, and integration outweigh the need for extreme force output. We further demonstrate that our PVDF actuators can achieve **over 3 mm of free deflection, 20 mN of blocked force, and bandwidths exceeding 500 Hz**, while operating at voltages as low as 150 V. Finally, to illustrate their potential for robotic integration, we present a planar translating micro-robot driven by resonant PVDF actuation, achieving robust and controllable locomotion. In summary, the contributions of this work are:

- (1) a multilaminate stacking architecture that distributes a parallel electrical drive across each PVDF layer;
- (2) experimental validation that actuator performance scales predictably with layer number and geometry; and
- (3) demonstration of PVDF multilaminate actuators in a robotic platform, bridging the performance gap between brittle high-force ceramic actuators and compliant low-bandwidth soft polymer actuators.

II. MODELING AND CHARACTERIZATION EQUATIONS

A. Unimorph Composite Beam Model

A unimorph PVDF actuator (an active piezoelectric layer bonded to one side of a passive stiffening layer) can be modeled as a composite Euler–Bernoulli beam with the multilayer piezoelectric stack on top of the stiffening layer, as shown in figure 2. In this configuration, the actuator generates an actuation moment in only one bending direction when voltage is applied. Extending the concept to a bimorph—by adding a second piezoelectric stack beneath the stiffening layer—would enable bidirectional bending, but only unimorph configurations were fabricated and tested in this work.

The adhesive layers were neglected for clarity in this analytical derivation; however, they were included in the complete composite model used to fit the theoretical predictions to experimental data. Inclusion of these layers modifies Eqn 3, 4, and 5 by introducing additional non-active thickness and elastic compliance into the stack.

Both the blocked force and the free displacement of the actuator depend on the actuation bending moment M_{act} as given in Eqn 1 and 2.

$$F_{\text{blocked}} = \frac{3 M_{\text{act}}}{2L} \quad (1)$$

where F_{blocked} is the blocked force at the actuator tip (N), M_{act} is the actuation bending moment (N·m), and L is the beam length (m).

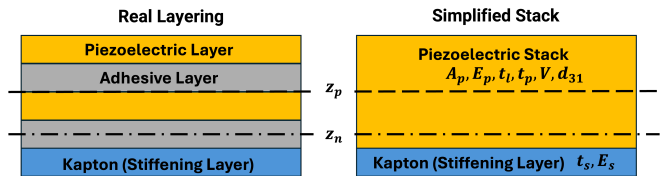


Fig. 2: Cross-sectional view of the unimorph piezoelectric actuator and its simplified beam model. t_p , t_ℓ , and t_s are the thicknesses of the piezostack, individual piezoelectric layers, and stiffening layer, respectively. A_p is the cross-sectional area of the piezostack. z_p and z_n are the centroid of the piezostack and neutral axis. E_p and E_s are the Young’s moduli of the piezostack and stiffening layer. V is the applied voltage across the piezostack, and d_{31} is the transverse piezoelectric coefficient of the PVDF layers.

$$\delta_{\text{free}} = \frac{L^2}{2} \frac{M_{\text{act}}}{EI_{\text{eq}}} \quad (2)$$

where δ_{free} is the free (unloaded) tip displacement (m) and EI_{eq} is the equivalent flexural stiffness of the composite beam (N·m²).

Since the piezostack is made up of multiple layers, the geometry of the beam is defined by eq. 3 and eq. 4.

$$t_p = N t_\ell, \quad A_p = b t_p \quad (3)$$

where t_p is the total piezostack thickness (m), N is the number of active layers, t_ℓ is the thickness of one piezoelectric layer (m), A_p is the cross-sectional area of the piezostack (m²), and b is the beam width (m).

$$z_n = \frac{E_s A_s z_s + E_p A_p z_p}{E_s A_s + E_p A_p}, \quad A_s = b t_s \quad (4)$$

where z_n is the neutral axis position (m), E_s and E_p are the Young’s moduli (Pa) of the substrate and piezoelectric layers, respectively, A_s is the cross-sectional area of the substrate (m²), t_s is the substrate thickness (m), and z_s , z_p are the centroids of the substrate and piezoelectric layers (m).

The flexural stiffness of the beam is determined by eq. 5.

$$EI_{\text{eq}} = E_s (I_s + A_s (z_s - z_n)^2) + E_p (I_p + A_p (z_p - z_n)^2) \quad (5)$$

where $I_s = \frac{b t_s^3}{12}$ and $I_p = \frac{b t_p^3}{12}$ are the second moments of area (m⁴) of the substrate and piezoelectric layers about their centroids.

The actuation moment is dependent on these quantities as in eq. 7 as well as ϵ^* which is defined in eq. 6.

$$\epsilon^* = d_{31} \frac{V}{t_\ell} \quad (6)$$

where ϵ^* is the free piezoelectric strain, d_{31} is the transverse piezoelectric coefficient (m/V), and V is the applied voltage (V).

$$M_{\text{act}} = E_p A_p \epsilon^* (z_p - z_n) \quad (7)$$

Combining these equations yields the simplified analytical relationships for blocked force and free displacement (Eqn

8 and 9). These expressions capture the primary electromechanical coupling behavior and are used for interpretation, while the full multilayer model—including adhesive and interfacial layers—is employed for quantitative comparison to experimental data.

$$F_{\text{blocked}} = \frac{3 E_p b N d_{31} V (z_p - z_n)}{2 t_\ell L} \quad (8)$$

$$\delta_{\text{free}} = \frac{L^2 E_p b N d_{31} V (z_p - z_n)}{2 t_\ell E I_{\text{eq}}} \quad (9)$$

B. Blocked Force and Force–Displacement Tradeoff

As shown in eq. 8 and 9, both the blocked force and the free displacement are proportional to $\frac{d_{31} V}{t_\ell}$, indicating that higher voltages, thinner layers, and larger piezoelectric coefficients improve the overall mass-normalized power density of the actuator. However, the remaining terms reveal a tradeoff between displacement and force. This tradeoff arises from the flexural stiffness term in the denominator of the free displacement expression. Since $I \propto b h^3$, increasing the total beam thickness dramatically reduces the achievable free displacement. In contrast, the blocked force scales roughly linearly with the number of active layers N because the dominant changing parameters are N and $(z_p - z_n)$. However, since the elastic modulus of PVDF is much lower than that of Kapton, $(z_p - z_n)$ remains nearly constant for small numbers of layers. This intrinsic tension between force generation and displacement amplitude defines the actuator’s optimal geometry for maximizing mass-specific power output, allowing designs to be tuned for application-specific requirements without relying on mechanical amplification mechanisms.

C. Resonance and Bandwidth

For dynamic operation, the first bending resonance frequency of a clamped-free unimorph is approximated by:

$$f_1 \approx \frac{1.875^2}{2\pi L^2} \sqrt{\frac{(EI)_{\text{eq}}}{\rho_{\text{eq}} A}}, \quad (10)$$

where $\rho_{\text{eq}} A$ is the mass per unit length of the laminate. Operating at resonance yields a Q-factor amplification of displacement:

$$w_{\text{tip, res}} \approx Q \cdot w_{\text{tip, static}}. \quad (11)$$

Previous studies indicate that PVDF actuators can show $Q \sim 10$ – 15 depending on substrate and bonding [17], enabling up to order-of-magnitude increases in displacement when driven at resonance. We intend to exploit this property in our design for robotics applications using lightweight actuators at resonance for high-performance efficient locomotion.

D. Characterization of Energy and Power Density

The mechanical work output of the actuator during cyclic operation is defined as

$$W = \int_{t_0}^{t_f} \vec{F} \cdot \vec{v} dt \quad (12)$$

where \vec{F} is the instantaneous tip force generated by the actuator, \vec{v} is the instantaneous tip velocity, and t_0 and t_f are the initial and final times of the actuation cycle, respectively.

In the loaded displacement experiments, each actuator was driven sinusoidally at a prescribed frequency and voltage amplitude while lifting a known mass m_{load} . The corresponding displacement curves were recorded and numerically differentiated to obtain instantaneous velocity and acceleration profiles. The product $\vec{F} \cdot \vec{v}$ was then integrated over one cycle to yield the mechanical work output W . The average mechanical power was computed as

$$P = \frac{W}{t_f - t_0}. \quad (13)$$

To allow meaningful comparison with other soft actuators and robotic systems, both the work and power were normalized by the total actuator mass m_{act} , giving the specific (mass-normalized) energy and power densities:

$$w = \frac{W}{m_{\text{act}}}, \quad p = \frac{P}{m_{\text{act}}}. \quad (14)$$

These quantities represent the actuator’s ability to deliver mechanical energy and power relative to its own weight, providing a direct measure of performance relevant for mobile or weight-limited robotic applications.

III. SCALABLE LAMINATE FABRICATION

A. Manufacturing Considerations

Fabricating multilaminar PVDF actuators presents several nontrivial challenges due to the combination of small feature sizes, operating voltages, and the thermal sensitivity of the material. As multilayer PVDF actuators are a recent development, new manufacturing techniques were required to achieve repeatable, robust, and scalable designs. The most critical challenges and their corresponding solutions are discussed below.

1) Electrode Design

Because the individual actuator layers are on the order of tens of micrometers thick and operate at voltages of hundreds of volts, electrical shorting becomes a primary limitation in multilaminar architectures. The breakdown voltage of air gaps and adhesive interlayers is insufficient to prevent dielectric failure when the positive electrode of one layer is positioned directly adjacent to the negative electrode of its neighbor. To address this, we implemented an *asymmetric stacking architecture* (Fig. 3) in which each electrode is neighbored by one of the same polarity. This configuration allows all positive electrodes to be routed to one side of the actuator and all negative electrodes to the opposite side, where they are collectively bonded using silver epoxy. This arrangement eliminates interlayer shorting while maintaining a simple and scalable electrical interface.

2) Thermal Depoling

PVDF and its copolymers depole rapidly when exposed to temperatures near or above their Curie point ($\sim 100^\circ\text{C}$). Conventional lamination processes, which often rely on heat

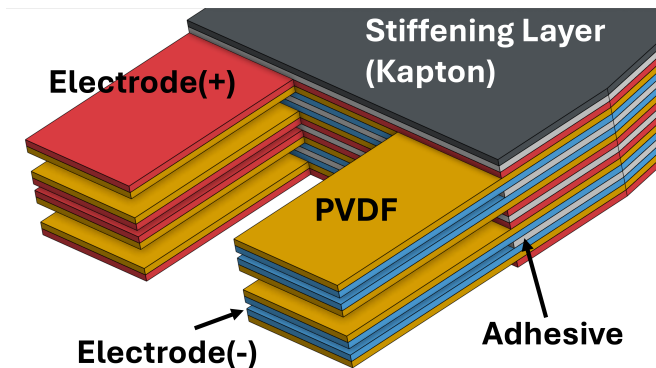


Fig. 3: Schematic of the asymmetric electrode layout used to prevent interlayer shorting in multilaminated PVDF actuators. All positive electrodes are routed to one side of the stack, and all negative electrodes to the other, enabling reliable electrical connection with silver epoxy.

bonding or hot pressing, therefore risk degrading piezoelectric performance. To avoid thermal depoling, the multilayer stacks were fabricated entirely at room temperature using a thin-film Nitto adhesive to bond each layer. This approach preserved the polarization state of the PVDF films while ensuring consistent interfacial adhesion and layer alignment.

B. PVDF Film Choice and Preparation

PVDF's piezoelectricity originates from its polar β -phase (all-trans conformation), which is stabilized through mechanical stretching and electrical poling. For this work, we used commercially available uniaxially oriented PVDF films (PolyK Technologies) with thicknesses $t_\ell \in \{7, 12\} \mu\text{m}$. These films are pre-stretched to promote β -phase content and supplied in a poled state, ensuring consistent electromechanical properties across batches.

Film thickness was chosen as a key design variable for evaluating scaling behavior. Thinner films experience a higher electric field for the same applied voltage, according to $E = V/t_\ell$, resulting in proportionally greater actuation strain and, consequently, higher mass-normalized power density. In contrast, thicker films provide greater flexural stiffness but lower field strength for a given voltage. This tradeoff is reflected in the experimental results presented later in this work.

C. Electrode Deposition and Patterning

Two electrode deposition strategies were investigated:

- 1) **Laser rastering of pre-coated films:** A 6D Laser Micromachine femtosecond laser (Light Conversion Carbide-CB5) was used to ablate unwanted electrode regions from pre-metallized PVDF [18], [19]. While functional, small variations in electrode thickness reduced repeatability, and local heating due to large area ablation caused thermal damage to the PVDF.
- 2) **Sputter coating through shadow masks:** Bare PVDF films were masked and sputtered with gold electrodes (figure 4). This approach provided uniform coverage,

batch scalability, and flexibility to define asymmetric electrode geometries for alternating-layer stacks.

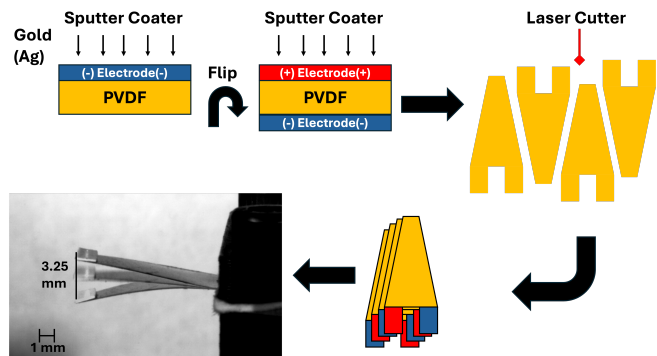


Fig. 4: Actuator manufacturing process

Electrode material choice affects scalability and durability. Brittle, thick-film metals can crack under cyclic bending, while compliant materials such as gold mesh, silver nanowires, PEDOT:PSS, graphene inks, etc. extend lifetime at high curvature in future iterations. Ink printing might be an especially strong choice for batch processing of actuator layers.

D. Lamination and Stacking

Unimorph and multilayer PVDF actuators were fabricated by laminating individual PVDF films with a thin adhesive layer at room temperature. This process avoids exceeding PVDF's Curie temperature ($\sim 100^\circ\text{C}$), thereby preserving the polarization state of each film. The adhesive layer thickness was minimized to a few microns to reduce interfacial compliance and shear lag, which otherwise dissipate strain energy and lower the effective electromechanical coupling efficiency.

A polyimide (Kapton) sheet was used as the passive stiffening substrate due to its moderate stiffness and good adhesion to the nitto adhesive. Compared to stiffer materials such as carbon fiber, Kapton provides a favorable balance between output force and tip displacement.

Finally, the alternating electrode architecture allows all PVDF layers to be driven in parallel, such that each film experiences the full electric field. This configuration simplifies electrical connection, scales output force approximately linearly with the number of layers, and maintains low operating voltage per layer.

E. Integration into Robotic Systems and Scalability

A key advantage of PVDF laminates is their compatibility with low-temperature, scalable fabrication. Roll-to-roll sputter coating, tape lamination, and low-cost patterning (inkjet, stencil, screen printing) are all feasible for future large-scale production. The thin-film nature of PVDF also allows direct integration into robot structures, such as morphing skins, legs, or appendages.

IV. ACTUATOR PERFORMANCE

A. Experimental Setup

The tip position of each actuator was measured using a time-of-flight (ToF) laser (Keyence LK-HD500), while blocked force was recorded with a force sensor (LSB200, Futek). A high-speed Phantom V720 camera was used concurrently to verify tip deflection measurements and to ensure minimal out-of-plane twisting. Data acquisition was performed in real time using a Speedgoat computer.

Each actuator was subjected to three loading conditions: free displacement, blocked force, and loaded displacement. A frequency chirp was applied to determine the resonant frequency under each condition. Subsequently, each actuator was tested using both a pseudo-static signal (5 Hz) and at resonance to assess performance under dynamic conditions.

B. Static Displacement and Force Measurements

Actuators were tested using PVDF films of thickness $t_\ell \in \{7, 12\} \mu\text{m}$, assembled into 4- and 8-layer stacks. A laser displacement sensor was used to track free tip deflection, and a force transducer measured blocked tip force.

Displacement: $7 \mu\text{m}$ films produced approximately $2\times$ greater free displacement than $12 \mu\text{m}$ films at the same drive voltage, consistent with higher electric field for thinner films. For 10 mm beams, free tip deflections of up to 1 mm were measured.

Force: $12 \mu\text{m}$ films produced $\sim 25\%$ higher blocked force than $7 \mu\text{m}$ films at the same drive voltage. As predicted, blocked force scaled approximately linearly with the number of layers ($F \propto N$). Under static conditions, the maximum blocked forces of 1.8 mN were achieved with 8-layer stacks.

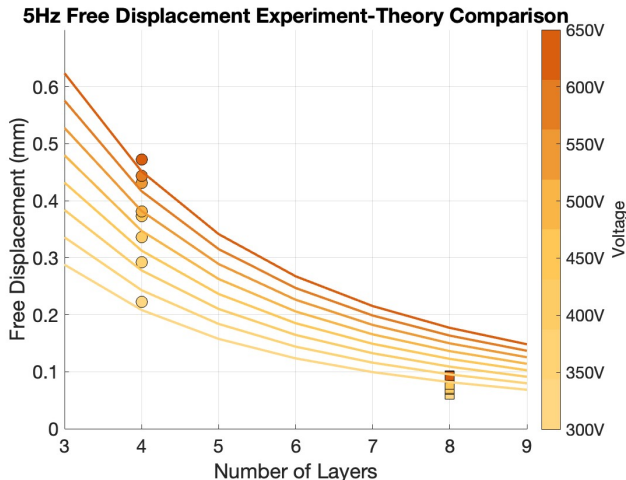


Fig. 5: Comparison between theoretical and experimental displacement

C. Actuator Performance Characterization

Actuator performance was evaluated through loaded displacement tests, where a small mass (a strip of gel pack) was attached to the actuator tip and the resulting displacement was recorded. Both static and resonant conditions were

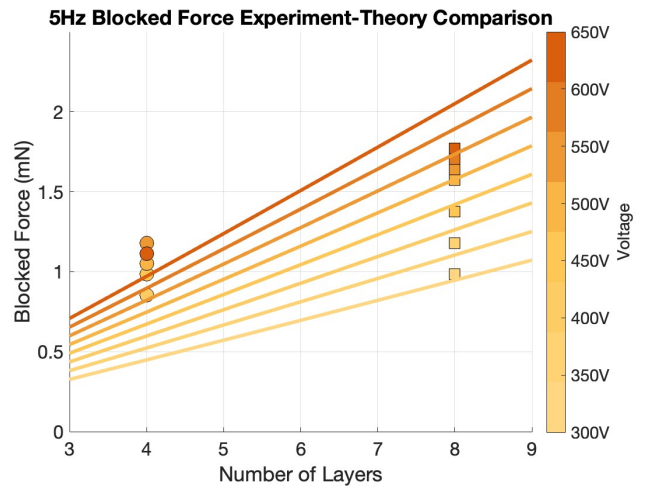


Fig. 6: Comparison between theoretical and experimental blocked force

tested to characterize quasi-static and dynamic responses, respectively. Data were collected in real time using the Speedgoat system.

For consistency with standard practices in dielectric elastomer actuator (DEA) characterization, all reported power density values correspond to resonant operation, which represents the highest achievable mechanical output and minimizes the effects of viscoelastic damping. Operating at resonance also aligns the comparison with other soft actuator studies in literature.

Fig. 7 shows the normalized power density of actuators fabricated with $7 \mu\text{m}$ and $7 \mu\text{m}$ PVDF films. The $7 \mu\text{m}$ actuators consistently demonstrated superior normalized power density due to the higher electric field attainable across thinner layers at the same driving voltage. The maximum measured value reached approximately 40 W/kg at 450 V , which is comparable to widely used PZT actuators. It was also achieved at significantly lower operating voltage than typical DEAs or HASEL actuators. This represents a meaningful step toward compact, low-voltage, high-performance piezoelectric soft actuators.

V. ROBOTIC DEMONSTRATIONS

A. PVDF Tripod Platform

To demonstrate the feasibility of multilayer PVDF actuators in robotic systems, we constructed *PVDF Tripod*, a planar triangular microrobot. Three multilayer PVDF actuators were mounted at 120° intervals around a lightweight triangular chassis (side length $\sim 4 \text{ cm}$, mass $\sim 117 \text{ mg}$). Each actuator operated as a bending unimorph, directly contacting the ground to produce locomotion. The design exploited the compliance of PVDF actuators, which allowed integration without rigid mechanical amplification mechanisms.

B. Locomotion Performance

PVDF Tripod was actuated by sinusoidal voltage waveforms delivered in-phase to two of the three actuators.

Property	PVDF piezo	PZT H5	DEA	HASEL
Mass	15 mg	125 mg [4]	100 mg [20]	10 g [10]
Voltage	300 V	300 V [21]	0.2–6 kV [22]	0.2–8 kV [23]
Frequency	100–500 Hz	5–300 Hz [18]	300–500 Hz [22]	0.1–40 Hz [23]
Displacement	3 mm	0.9 mm [21]	–	–
Force	20 mN	320 mN [5]	–	–
Power Density	40 W/kg	40 W/kg [24]	0.5–2 kW/kg [25]	100–600 W/kg [23]

TABLE I: Comparison of various soft electrically driven actuators. Missing data is indicated by “–”.

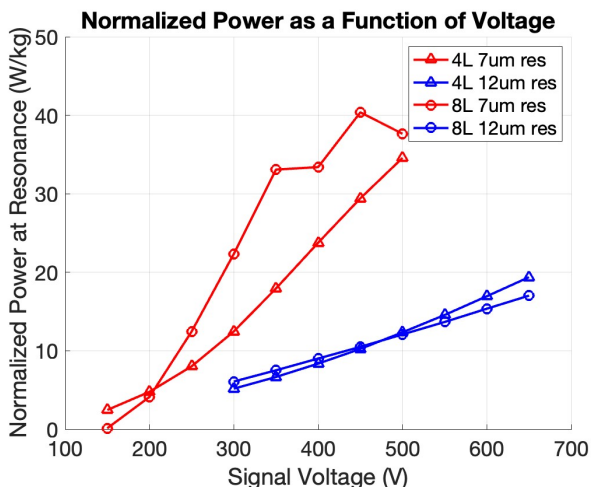


Fig. 7: Normalized mass power density for 7 μm and 12 μm PVDF actuators measured at resonance. Thinner (7 μm) films achieved higher power due to larger electric field strengths.

At low-frequency drive (< 100 Hz), the robot achieved stepwise hopping and inching motions, but displacements per cycle were small due to limited off-resonance deflection. At resonance drive (~ 200 Hz), actuator tip deflection increased by up to $10\times$, enabling continuous locomotion, and PVDF Tripod reached forward speeds of several mm/s (~ 0.15 body lengths/s).

C. Robustness to Perturbations

PVDF’s mechanical toughness and compliance provided robustness advantages in robotic contexts: the actuators sustained repeated collisions and ground impacts without fracture, unlike brittle PZT actuators; the PVDF Tripod retained locomotion capability even after lateral perturbations such as pokes and tilts, self-stabilizing due to resonance-driven oscillations; and the actuators continued to function even after being crushed by a large (500 g) weight (Figure 8).

D. Comparative Robotics Perspective

Compared to robots driven by PZT actuators, PVDF Tripod exhibits lower thrust but dramatically higher robustness and resilience to shocks. Compared to DEA- or HASEL-driven robots, PVDF Tripod offers higher bandwidth (> 500 Hz) and thinner, more easily integrated actuators, at the cost of lower strain. This positions PVDF-actuated microrobots as a middle ground: capable of resonant locomotion in cluttered environments where durability and lightweight design outweigh maximum force density.

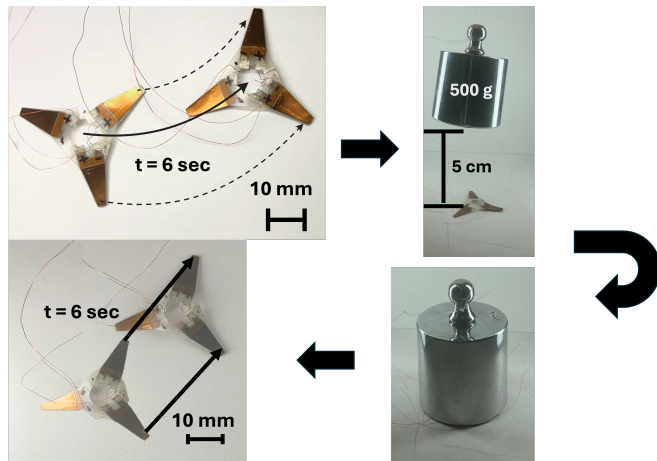


Fig. 8: PVDF Tripod locomotion before and after crushing

E. Future Robotic Applications

Looking forward, multilayer PVDF actuators can be extended to legged microrobots using PVDF as flexural leg actuators for cockroach-inspired designs, aerial morphing through wing camber and twist modulation for insect-scale flying robots, haptic interfaces and skins that provide conformal, lightweight actuators for wearable robotics, and distributed actuation in which lightweight, strain-based actuation is spread across the robot body to take better advantage of innate dynamics. These examples highlight PVDF’s potential to expand the actuation toolbox for physical intelligence and distributed actuation in microrobotic systems.

ACKNOWLEDGMENT

We thank all the members of the Animal Inspired Movement and Robotics Lab at the University of Colorado Boulder for their valuable support and suggestions with the robot design and testing.

REFERENCES

- [1] K. Y. Ma, P. Chirarattananon, S. B. Fuller, and R. J. Wood, “Controlled Flight of a Biologically Inspired, Insect-Scale Robot,” *Science*, vol. 340, pp. 603–607, May 2013. Publisher: American Association for the Advancement of Science.
- [2] Y. M. Chukewad, J. James, A. Singh, and S. Fuller, “RoboFly: An Insect-Sized Robot With Simplified Fabrication That Is Capable of Flight, Ground, and Water Surface Locomotion,” *IEEE Transactions on Robotics*, vol. 37, pp. 2025–2040, Dec. 2021. Conference Name: IEEE Transactions on Robotics.
- [3] B. Goldberg, N. Doshi, K. Jayaram, J.-S. Koh, and R. J. Wood, “A high-speed motion capture method and performance metrics for studying gaits on an insect-scale legged robot,” in *2017 IEEE/RSJ International Conference on Intelligent Robots and Systems (IROS)*, (Vancouver, BC), pp. 3964–3970, IEEE, Sept. 2017.

- [4] H. Kabutz and K. Jayaram, "Design of CLARI: A Miniature Modular Origami Passive Shape-Morphing Robot," *Advanced Intelligent Systems*, vol. 5, no. 12, p. 2300181, 2023.
- [5] H. Kabutz, A. Hedrick, W. P. McDonnell, and K. Jayaram, "mCLARI: A Shape-Morphing Insect-Scale Robot Capable of Omnidirectional Terrain-Adaptive Locomotion in Laterally Confined Spaces," in *2023 IEEE/RSJ International Conference on Intelligent Robots and Systems (IROS)*, (Detroit, MI, USA), pp. 8371–8376, IEEE, Oct. 2023.
- [6] N. Snis, E. Edqvist, U. Simu, and S. Johansson, "Monolithic fabrication of multilayer p(vdf-trfe) cantilevers," *Sensors and Actuators A: Physical*, vol. 144, no. 2, pp. 314–320, 2008.
- [7] S. Ahmed, Z. Ounaies, and E. A. F. Arrojado, "Electric field-induced bending and folding of polymer sheets using p(vdf-trfe-ctfe) terpolymer," *Sensors and Actuators A: Physical*, vol. 260, pp. 68–80, 2017.
- [8] Z. Ren, S. Kim, X. Ji, W. Zhu, F. Niroui, J. Kong, and Y. Chen, "A High-Lift Micro-Aerial-Robot Powered by Low-Voltage and Long-Endurance Dielectric Elastomer Actuators," *Advanced Materials*, vol. 34, p. 2106757, Feb. 2022.
- [9] N. Kellaris, V. Gopaluni Venkata, G. M. Smith, S. K. Mitchell, and C. Keplinger, "Peano-HASEL actuators: Muscle-mimetic, electrohydraulic transducers that linearly contract on activation," *Science Robotics*, vol. 3, p. eaar3276, Jan. 2018. Publisher: American Association for the Advancement of Science.
- [10] E. Acome, S. K. Mitchell, T. G. Morrissey, M. B. Emmett, C. Benjamin, M. King, M. Radakovitz, and C. Keplinger, "Hydraulically amplified self-healing electrostatic actuators with muscle-like performance," *Science*, vol. 359, pp. 61–65, Jan. 2018.
- [11] C. M. Costa, R. Gonçalves, and S. Lanceros-Méndez, "Smart and multifunctional materials based on electroactive polymers," *Chemical Reviews*, vol. 123, no. 20, pp. 12364–12475, 2023.
- [12] Y. Wu, J. K. Yim, J. Liang, Z. Shao, M. Qi, J. Zhong, Z. Luo, X. Yan, M. Zhang, X. Wang, R. S. Fearing, R. J. Full, and L. Lin, "Insect-scale fast moving and ultrarobust soft robot," *Science Robotics*, vol. 4, p. eaax1594, July 2019.
- [13] A. S. Fiorillo, "Design and characterization of a pvdf ultrasonic range sensor," *EEE Transactions on Ultrasonics, Ferroelectrics, and Frequency Control*, 1992.
- [14] S. A. Rios and A. J. Fleming, "A new electrical configuration for improving the range of piezoelectric bimorph benders," *Sensors and Actuators A: Physical*, vol. 224, pp. 106–110, 2015. Publisher: Elsevier.
- [15] N. T. Jafferis, M. Lok, N. Winey, G.-Y. Wei, and R. J. Wood, "Multilayer laminated piezoelectric bending actuators: design and manufacturing for optimum power density and efficiency," *Smart Materials and Structures*, vol. 25, p. 055033, May 2016.
- [16] N. T. Jafferis, K. Jayaram, P. A. York, and R. J. Wood, "A streamlined fabrication process for high energy density piezoelectric bending actuators," *Sensors and Actuators A: Physical*, vol. 332, p. 113155, Dec. 2021.
- [17] F. J. Maier, *Flexoelectricity in PVDF and TiOx thin films: material characterization for MEMS applications*. PhD thesis, Technische Universität Wien, 2023.
- [18] H. Kabutz and K. Jayaram, "Integrated proprioceptive piezoelectric actuators for miniature robots and devices," *Smart Materials and Structures*, vol. 34, p. 035004, Feb. 2025. Publisher: IOP Publishing.
- [19] S. Lee, E. V. Bordatchev, and M. J. F. Zeman, "Femtosecond laser micromachining of polyvinylidene fluoride (PVDF) based piezo films," *Journal of Micromechanics and Microengineering*, vol. 18, p. 045011, Apr. 2008.
- [20] Y. Chen, H. Zhao, J. Mao, P. Chirattananon, E. F. Helbling, N.-s. P. Hyun, D. R. Clarke, and R. J. Wood, "Controlled flight of a microbot powered by soft artificial muscles," *Nature*, vol. 575, pp. 324–329, Nov. 2019. Publisher: Nature Publishing Group.
- [21] N. T. Jafferis, M. J. Smith, and R. J. Wood, "Design and manufacturing rules for maximizing the performance of polycrystalline piezoelectric bending actuators," *Smart Materials and Structures*, vol. 24, p. 065023, June 2015.
- [22] Z. Ren, S. Kim, X. Ji, W. Zhu, F. Niroui, J. Kong, and Y. Chen, "A high-lift micro-aerial-robot powered by low-voltage and long-endurance dielectric elastomer actuators," *Advanced Materials*, vol. 34, no. 7, p. 2106757, 2022.
- [23] X. Wang, S. K. Mitchell, E. H. Rumley, P. Rothmund, and C. Keplinger, "High-strain peano-hasel actuators," *Advanced Functional Materials*, vol. 30, no. 7, p. 1908821, 2019.
- [24] Z. Li, R. Zhu, X. Yi, and S. Dong, "A high-power-density piezoelectric actuator operating in bicycling movement mechanism," *IEEE Transactions on Industrial Electronics*, vol. 70, no. 6, pp. 6090–6098, 2023.
- [25] W. Feng, L. Sun, Z. Jin, L. Chen, Y. Liu, H. Xu, and C. Wang, "A large-strain and ultrahigh energy density dielectric elastomer for fast moving soft robot," *Nature Communications*, vol. 15, no. 1, p. 4222, 2024.